



Research Paper

# Mathematical Model of Fluid Flow and Solute Transport in Converging-diverging Permeable Tubes

M. Varunkumar<sup>1</sup> , P. Muthu<sup>2</sup> , S. Srinivas<sup>1</sup> 

<sup>1</sup> Department of Mathematics, School of Advance Sciences, VIT-AP University, Amaravati-522237, Andhra Pradesh, India

<sup>2</sup> Department of Mathematics, National Institute of Technology, Warangal-506004, Telangana State, India

Received September 06 2022; Revised February 07 2023; Accepted for publication February 07 2023.

Corresponding author: M. Varunkumar (varunkumar.merugu@vitap.ac.in)

© 2023 Published by Shahid Chamran University of Ahvaz

**Abstract.** This article presents a mathematical model for fluid and solute transport in an ultra-filtered glomerular capillary. Capillaries are assumed to be converging-diverging tubes with permeable boundaries. According to Starling's hypothesis, ultrafiltration is related to the variations in hydrostatic and osmotic pressures in the capillary and Bowman's space and takes place along the length of the capillary. The governing equations of fluid flow for the case of axisymmetric motion of viscous incompressible Newtonian fluid have been considered along with the solute transfer equation. The non-uniform geometry has been mapped into a finite regular computational domain via a coordinate transformation. Correspondingly, the governing equations are transformed to the computational space and solved to get the velocity and pressure values. The solute transfer equation is also solved numerically using a finite difference scheme. The solutions provide the predictions of the axial distribution of hydrostatic pressure and osmotic pressure, velocities, and concentration profiles at various points along the axis and solute clearance quantities along the capillary. The current results are in good agreement with the earlier findings in limiting cases of cylindrical tubes with a constant radius. It is found that there is a significant effect of osmotic pressure on the solute concentration. Using a set of data, the influence of various physiological parameters on the velocity components and solute concentration are presented and discussed through graphs to correlate with physiological situations. The generic structure of the current model also provides an acceptable approach to exploring fluid exchange in organs apart from the glomerular capillary.

**Keywords:** Glomerular capillary; Finite difference method; Ultrafiltration; Converging-diverging tubes; Permeable wall.

## 1. Introduction

The concentration of different chemical species in the blood, and hence throughout the body, is mostly regulated by the kidneys. A kidney's typical job is to eliminate metabolic waste products from the body. A concentration of blood cells and proteins on one side of the glomerular capillary wall and a solution of small molecules and ions, including waste products, on the other are the results of the glomerulus' filtering of blood. A capillary membrane separates the two streams coming from the glomerulus so that they pass simultaneously. This capillary membrane structure's special ability to actively convey sodium and other essential substances back into the concentrated blood stream makes it a standout among other structures. This membrane modifies the blood's water and salt content to the appropriate amount, and the residual ultrafiltrate turns into urine. In general, solutes are carried across the capillary membrane by convection and diffusion, and filtration process is controlled by Starling's hypothesis (i.e., ultrafiltration velocity is proportional to transboundary pressure differences). To preserve the composition of bodily fluids, nearly all of the ultrafiltrate is reabsorbed into the blood stream ([1-5]). As a result, understanding the function of nephrons can benefit greatly from research on solute transport in glomerular capillaries.

Glomerular filtration is mostly a passive process that is directly correlated with the intraglomerular hydrostatic pressure since it depends on the equilibrium of hydrostatic and osmotic pressures. As stated in Brenner et al. [6, 7], it is reasonable to anticipate a correlation between arterial blood pressure and the percentage of plasma filtrate driven through Bowman's region. The driving forces that cause the net transport through capillary walls can be of two different types: (1) changes in the fluids' hydrostatic and oncotic/osmotic pressures, and (2) variations in concentration of penetrating solutes on either side ([8-11]). The relationship between osmosis and diffusion in biological membranes was studied using a generalized transport equation that Kedem and Katchalsky [12] developed that included both of them.

The relationship between the ultrafiltrate flow and the variations of the micro vascular hydraulic and osmotic pressures is used in Deen et al. [13] model to explain how the protein concentration varies in the rat glomerular capillary. By assuming that the pressure gradient is constant along the capillary length, they were able to use a quadratic expression to associate the concentration of protein to its osmotic pressure. The mathematical model developed by Marshal and Trowbridge [14] considered axial distance as a factor affecting intraluminal pressure gradient and flow rate in a glomerular capillary. A study of the effect of capillary wall permeability on ultrafiltration by Papenfuss and Gross [15] extends Marshal and Trowbridge [14].



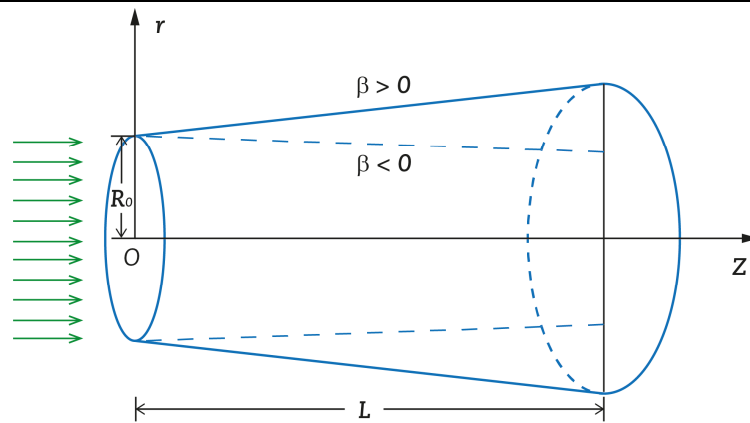


Fig. 1. Physical model of the glomerular capillary (Converging-diverging tube).

The authors of the aforementioned investigations have not taken into account the solutes' motion through the capillary wall, which is highly realistic and important in physiological processes (Martin et al. [8] and Guyton [5]). By assuming equal concentrations at each cross-section, Papenfuss and Gross [16] and Salathe [17] examined at the exchange of fluid and the flow of solute through the wall. By taking plasma protein transport through glomerular capillaries in which the wall of the capillaries acts as an impermeable barrier to species with constant hydrostatic pressure, Deen et al. [18] found both radial and axial concentration profiles. The work of Ross [19] investigated mass movement through a porous tube with Newtonian fluid on the assumption that permeable walls have radial velocity proportional to pressure differences. By considering the ultrafiltration velocity at the transmembrane, Tyagi and Abbass [20] developed a model of the uremic solute transport in an artificial kidney. Both the hydrostatic and osmotic pressures affect the membrane filtration velocity and mass movement inside the wall and across it. The glomerular filtration rate is also influenced by changes in the hydrostatic and colloidal osmotic pressures, as indicated by Chaturani and Ranganatha [21], and diffusion and convection are the two mechanisms that move solutes across the capillary. A computational model describing the transfer of water and solute water from Bowman space to the papillary end of a human kidney's nephron was developed by Layton and Layton [22]. They performed simulations to determine how much filtered water and soluble compounds are delivered via each unique and functionally diverse glomerular section using this approach. Pstras et al. [23] examined the transcappillary transport mechanisms on the whole-body level utilizing the three different pore concepts of the capillary wall (large, tiny, and ultra-small pores). Human blood plasma and interstitium, which are separated by capillary walls, are examples of simple and complicated systems for which Waniewski et al. [24] have presented examples of how to calculate the ion concentrations. Radhakrishnamacharya et al. [25] developed a mathematical model to investigate the effect of slip on the fluid and solute transport in a permeable channel. Recent studies of various physiological problems in regard to the glomerular capillaries can also be referred from the research articles (Varunkumar and Muthu [26, 27]).

The majority of the research mentioned above have studied glomerular capillary as a uniform tube. There is no doubt that it is idealized. It is stated that each glomerulus' filtration process occurs in different kidney regions has undergone some notable modification, with certain nephrons having a bigger volume than the other nephrons. Given that the surface area of the particular glomerular capillaries can vary, the conductivity and capillary surface area are crucial to the membrane filtration process (Martin et al. [8]). Hence, it is required to consider the effect of varying cross section of the capillary is more realistic in physiological situations. In order to analyze the flow via non-uniform shaped permeable tubes/channels and consider taking a first step toward understanding these problems, Radhakrishnamacharya et al. [28], Krishnaprasad and Chandra [29] and Chaturani and Ranganatha [30] considered the viscous fluid flow in a cylindrical tube of varying radius with permeable boundary.

According to the preceding review of the literature, there has never been a study of fluid flow and solute transport via non-uniform tube, as well as the presence of concentration dependency of osmotic pressure so far. The primary purpose of this research is to look at solute transport in a tube with a slowly changing cross section (convergent-divergent tubes) and a permeable boundary. Slope parameter, ultrafiltration parameter, diffusion coefficient, and transmittance coefficient are all taken into account. Analytical and numerical approaches are used to solve the flow equations, while an implicit finite difference technique is used to solve the solute transport equation. With the use of graphical findings, the profiles of hydrostatic, osmotic, velocity, and concentration distributions for the emerging parameters are illustrated and analyzed in detail. The mathematical model and the details of solution methodology are given below.

## 2. Mathematical Formulation

### 2.1. Governing Equations

Consider a steady solute transport in a fluid flow through a tube with length  $L$  and varying radius  $R(z)$ . An axisymmetric set-up by denoting axial and radial directions  $z$  and  $r$ , with corresponding axial velocity  $u(r, z)$  and radial velocity  $v(r, z)$  components is assumed. The equations governing such flow of viscous, incompressible, Newtonian fluid with constant viscosity ( $\mu$ ) and solute transport are:

$$\frac{\partial u}{\partial z} + \frac{\partial v}{\partial r} + \frac{v}{r} = 0 \quad (1)$$

$$v \frac{\partial u}{\partial r} + u \frac{\partial u}{\partial z} = -\frac{1}{\rho} \frac{\partial P}{\partial z} + \frac{\mu}{\rho} \left( \frac{\partial^2 u}{\partial z^2} + \frac{1}{r} \frac{\partial u}{\partial r} + \frac{\partial^2 u}{\partial r^2} \right) \quad (2)$$

$$v \frac{\partial v}{\partial r} + u \frac{\partial v}{\partial z} = -\frac{1}{\rho} \frac{\partial P}{\partial r} + \frac{\mu}{\rho} \left( \frac{\partial^2 v}{\partial z^2} + \frac{1}{r} \frac{\partial v}{\partial r} - \frac{v}{r^2} + \frac{\partial^2 v}{\partial r^2} \right) \quad (3)$$



$$v \frac{\partial c}{\partial r} + u \frac{\partial c}{\partial z} = D \left( \frac{1}{r} \frac{\partial c}{\partial r} + \frac{\partial^2 c}{\partial r^2} + \frac{\partial^2 c}{\partial z^2} \right) \tag{4}$$

where  $P$  is the pressure,  $\mu$  is the dynamic viscosity and  $\rho$  is the density.  $D$  and  $c$  are the diffusion coefficient and solute concentration, respectively.

**2.2. Boundary conditions**

The appropriate boundary conditions corresponding to equations (1) to (4) to model the solute transfer in a glomerular capillary are:

(i) at entrance ( $z = 0$ ) of the capillary:

$$c = c_0 \tag{5}$$

$$\Delta P = \Delta P_a \tag{6}$$

$$\int_0^{R_0} 2\pi r u(r, 0) dr = Q_0 \tag{7}$$

(ii) regularity condition (axial-symmetric),  $r = 0$ :

$$\frac{\partial c}{\partial r} = 0, \frac{\partial u}{\partial r} = 0, v = 0 \tag{8}$$

(iii) the solute mass flux, axial and radial velocity components at permeable wall  $r = R(z)$  ([18, 21, 30]):

$$-D \frac{\partial c}{\partial r} = h(c - c_T) + (T_R - 1) V_R \begin{cases} c; V_R > 0 \\ c_T; V_R < 0 \end{cases} \tag{9}$$

$$v = \frac{k(\Delta P - \sigma \Delta \pi)}{\sqrt{1 + \left(\frac{dR}{dz}\right)^2}} = V_R \tag{10}$$

$$u = \frac{-k(\Delta P - \sigma \Delta \pi) \frac{dR}{dz}}{\sqrt{1 + \left(\frac{dR}{dz}\right)^2}} \tag{11}$$

where  $\Delta P = P$  (hydrostatic pressure inside tube wall) -  $P_T$  (hydrostatic pressure outside tube wall),  $\Delta P_a = P_a$  (inlet hydrostatic pressure) -  $P_T$ ,  $\Delta \pi = \pi$  (osmotic pressure inside tube wall) -  $\pi_T$  (osmotic pressure outside tube wall),  $Q_0$  is the inlet volume flux, respectively.  $h$  is solute wall permeability,  $T_R$  is transmittance coefficient [32],  $k$  is hydraulic wall permeability, and  $\sigma$  is the reflection coefficient [31],  $c_0$  is inlet concentration of solute, and  $c_T$  is the concentration outside the tube.

The osmotic pressure increases as the protein concentration increases and the relation is given by [15]:

$$\pi(c) = b_1 c(R, z) + b_2 c(R, z)^2 + b_3 c(R, z)^3 \tag{12}$$

where  $b_1, b_2$  and  $b_3$  are constants.

The total solute mass flux  $J_s$  and total solute clearance  $J_c$  of the capillary are [31]:

$$J_s(z) = (c(R, z) - c_T)h + V_R T_R \begin{cases} c; V_R > 0 \\ c_T; V_R < 0 \end{cases} \tag{13}$$

$$J_c = \int_{z=0}^{z=L} \pi R J_s(z) dz \tag{14}$$

Here, we consider the geometry of the glomerular capillary tube (converging/diverging) as:

$$R(z) = R_0 [1 + (\beta / R_0)z], \quad 0 \leq z \leq L \tag{15}$$

where  $R_0$  is the radius of the tube at the entrance ( $z = 0$ ),  $\beta$  is the wall slope parameter, and  $L$  is the length of tube as represented in Fig. 1.

**3. Non-dimensionalisation**

We non-dimensionalise the equations by defining  $z = z^* R_0, r = r^* R_0, v = v^* U_0, u = u^* U_0, z = z^* R_0, r = r^* R_0, v = v^* U_0, u = u^* U_0, V_R = V_R^* U_0, c = c^* c_0, c_T = c_T^* c_0, \Delta P = \Delta P^* \Delta P_a, \Delta \pi = \Delta \pi^* \Delta P_a, b_1 = b_1^* (\Delta P_a / c_0), b_2 = b_2^* (\Delta P_a / c_0^2), b_3 = b_3^* (\Delta P_a / c_0^3), J_s = J_s^* (c_0 D / R_0), J_c = J_c^* (Q_0 c_0), Q = Q^* Q_0, Q_0 = \pi r^2 U_0$ .

According to [19], axial diffusion in capillary walls is less significant than radial diffusion. It is presumed that the tube length to diameter ratio is so great that there are no end effects. Additionally, since the net radial flow is much less than the typical



axial flow, inertial effects may be disregarded (Reynolds values are on the order  $10^{-3}$ ). Using these non-dimensional variables and assumptions, the governing equations (1) to (15) become (after dropping \*\*):

$$\frac{\partial u}{\partial z} + \frac{\partial v}{\partial r} + \frac{v}{r} = 0 \tag{16}$$

$$\frac{\partial(\Delta P)}{\partial z} = \frac{1}{R_p} \left( \frac{\partial^2 u}{\partial r^2} + \frac{1}{r} \frac{\partial u}{\partial r} \right) \tag{17}$$

$$\frac{\partial(\Delta P)}{\partial r} = 0 \tag{18}$$

$$v \frac{\partial c}{\partial r} + u \frac{\partial c}{\partial z} = \frac{1}{Pe} \left( \frac{\partial^2 c}{\partial r^2} + \frac{1}{r} \frac{\partial c}{\partial r} \right) \tag{19}$$

$$c = 1 \quad \text{at} \quad z = 0 \tag{20}$$

$$\Delta P = 1 \quad \text{at} \quad z = 0 \tag{21}$$

$$\int_0^1 2\pi r u(r, 0) dr = 1 \quad \text{at} \quad z = 0 \tag{22}$$

$$\frac{\partial c}{\partial r} = 0, \quad \frac{\partial u}{\partial r} = 0, \quad v = 0 \quad \text{at} \quad r = 0 \tag{23}$$

$$\frac{\partial c}{\partial r} = (c_T - c)Sh + (1 - T_R)PeV_R \begin{cases} c; V_R > 0 \\ c_T; V_R < 0 \end{cases} \quad \text{at} \quad r = R(z) \tag{24}$$

$$u = \frac{-\epsilon R_p (\Delta P - \sigma \Delta \pi) \beta}{\sqrt{1 + \beta^2}} \quad \text{at} \quad r = R(z) \tag{25}$$

$$v = \frac{\epsilon R_p (\Delta P - \sigma \Delta \pi)}{\sqrt{1 + \beta^2}} \quad \text{at} \quad r = R(z) \tag{26}$$

$$J_s(z) = Sh(c(R, z) - c_T) + PeT_R V_R \begin{cases} c(1, z); V_R > 0 \\ c_T; V_R < 0 \end{cases} \tag{27}$$

$$J_c = \frac{1}{Pe} \int_0^{\frac{L}{R}} J_s(z) dz \tag{28}$$

$$R(z) = 1 + \beta z \quad \text{for} \quad 0 \leq z \leq 1 \tag{29}$$

where  $Pe = U_0 R_0 / D$ ,  $Sh = hR / D$  and  $\epsilon = k\mu / R$  are the Peclet number, Sherwood number and ultrafiltration parameter, respectively. Here, the term  $R_p = R_0 \Delta P_a / \mu U_0$  does not have any physical meaning of interest, which expressed in eqns. (17), (25) and (26).  $U_0$  is the initial average velocity and  $Q$  is the flow rate.

### 4. Method of Solution

#### 4.1. Coordinate Transformation

The solutions of the equations (16) to (19) are difficult to find in closed form expressions due to the nonlinear and coupled behavior of velocity, and pressure components with solute concentration. Further, the non-uniformity of the physical domain poses a difficulty to solve these equations numerically, since discretization of this domain will give variable step size in radial direction at each cross section. So, we need to transform the non-uniform physical domain into uniform computational domain (shown in the Fig. 2), using the coordinate transformation (John [33]):

$$\xi = z, \quad \eta = \frac{r}{R(z)} \tag{30}$$

The above transformation maps the upper non-uniform boundary into a straight boundary. That is,  $r = 0$  and  $r = R(z)$  are mapped into  $\eta = 0$  and  $\eta = 1$ , respectively, in the computational domain. Accordingly, the governing equations for flow variables and solute concentration are also transformed. The flow field variables are computed at all grid points in the computational domain as in Fig. 2. The solutions of equations (16) and (17) for  $u$  and  $v$  re obtained as:



$$u(\xi, \eta) = \frac{R_p}{4} \frac{d\Delta P}{d\xi} R(\xi)^2 (\eta^2 - 1) - \epsilon R_p (\Delta P - \sigma \Delta \pi) \beta \sqrt{1 + \beta^2} \tag{31}$$

$$v(\xi, \eta) = \frac{R_p}{16} \frac{d^2 \Delta P}{d\xi^2} R(\xi)^2 [2\eta - \eta^3] + \frac{R_p}{4} \frac{d\Delta P}{d\xi} R(\xi)^2 \frac{dR}{dz} \eta + \frac{\epsilon R_p}{2} \left[ \frac{d\Delta P}{d\xi} - \sigma \frac{d\Delta \pi}{d\xi} \right] R(\xi) \eta \beta \sqrt{1 + \beta^2} \tag{32}$$

Equation (32) and boundary condition (26) determine the hydrostatic pressure equation as follows:

$$\frac{d^2 \Delta P}{d\xi^2} + B_1(\xi) \frac{d\Delta P}{d\xi} + B_2(\xi) \Delta P = B_3(\xi) \tag{33a}$$

where

$$B_1(\xi) = \frac{4\beta [R(\xi) + 2\epsilon \sqrt{1 + \beta^2}]}{(R(\xi))^2} \frac{d(\Delta P)}{d\xi}, B_2(\xi) = \frac{8\epsilon [-2\sqrt{1 + \beta^2}] \Delta P}{(R(\xi))^3}, B_3(\xi) = \frac{8\epsilon \sigma \beta \sqrt{1 + \beta^2}}{(R(\xi))^2} \frac{d(\Delta \pi)}{d\xi} - \frac{B_2(\xi) \sigma \Delta \pi}{\Delta P} \tag{33b}$$

The equations (21) and (22) will take the forms:

$$\Delta P = 1 \quad \text{at} \quad \xi = 0 \tag{34}$$

$$\frac{d\Delta P}{d\xi} = -\frac{8}{R_p R(\xi)^2} - \frac{8\epsilon(1 - \sigma \Delta \pi) \beta}{R(\xi)^2 \sqrt{1 + \beta^2}} \quad \text{at} \quad \xi = 0 \tag{35}$$

where

$$\Delta \pi = \pi - \pi_T = 0.009 [c(\xi, 1)^3 - c_T^3] + 0.16 [c(\xi, 1)^2 - c_T^2] + 2.1 [c(\xi, 1) - c_T]. \tag{36}$$

Now, the solute transfer equation (19) along with initial and boundary conditions (20), (23) and (24) are given in the new coordinate system  $(\xi, \eta)$ , as:

$$u \frac{\partial c}{\partial \xi} - \frac{\eta \beta}{R(\xi)} u \frac{\partial c}{\partial \eta} + \frac{1}{R(\xi)} v \frac{\partial c}{\partial \eta} = \frac{1}{Pe R(\xi)^2 \eta} \left[ \frac{\partial c}{\partial \eta} + \eta \frac{\partial^2 c}{\partial \eta^2} \right] \tag{37}$$

$$c = 1 \quad \text{at} \quad \xi = 0 \tag{38}$$

$$\frac{\partial c}{\partial \eta} = 0, \quad \frac{\partial u}{\partial \eta} = 0, \quad v = 0 \quad \text{at} \quad \eta = 0 \tag{39}$$

It is difficult to obtain closed form solutions analytically for the equations (33) and (37) that are related to hydrostatic pressure and concentration of solute. So, we obtain numerical solutions of (33) and (37) using corresponding boundary conditions (34), (35) and (38) to (40), respectively. The nonlinear differential equation (33) with boundary conditions (34) to (35) solved by using Runge-Kutta fourth order method.

### 4.2. Numerical Procedure

In order to determine the solute concentration, we must first solve equation (37), which is linked to equations (31), (32), (33) and (36). The equation (37) with the initial and boundary conditions (38) to (40) is solved by Crank-Nicolson finite difference scheme. Let  $i = 0$  and  $i = N$  represent the entrance and outflow of tube, respectively. Similarly,  $j = 0$  and  $j = M$  stand for the bottom and top, respectively. The increments in  $\xi$  and  $\eta$  directions are designated as  $\Delta \xi$  and  $\Delta \eta$ , respectively. The finite difference approach for equation (37) at a grid point  $(i, j)$ , can be written as, with reference to Fig. 2, as follows:

$$A_j c_{i+1,j-1} + B_j c_{i+1,j} + E_j c_{i+1,j+1} = R_j, \quad \text{for} \quad 0 \leq j \leq M, \quad 0 < i \leq N, \tag{40}$$

where

$$\begin{aligned} A_j &= \lambda(4\eta - 2\Delta\eta - Pe R(\xi) \beta \eta^2 (u_{i+1,j} + u_{i,j})) \Delta\eta + 2Pe R(\xi) \eta \Delta\eta v_{i+1,j}, \quad B_j = -4\eta(2\lambda + Pe R(\xi)^2 (u_{i+1,j} + u_{i,j})), \\ E_j &= \lambda(4\eta + 2\Delta\eta + Pe R(\xi) \beta \eta^2 (u_{i+1,j} + u_{i,j})) \Delta\eta - 2Pe R(\xi) \eta \Delta\eta v_{i+1,j}, \\ R_j &= \lambda(-4\eta + 2\Delta\eta + Pe R(\xi) \beta \eta^2 (u_{i+1,j} + u_{i,j})) \Delta\eta - 2Pe R(\xi) \eta \Delta\eta v_{i+1,j} c_{i,j-1} + 4\eta(2\lambda - Pe R(\xi)^2 (u_{i,j} + u_{i+1,j})) c_{i,j} \\ &\quad + \lambda(-4\eta - 2\Delta\eta - Pe R(\xi) \beta \eta^2 (u_{i,j} + u_{i+1,j})) \Delta\eta + 2Pe R(\xi) \eta \Delta\eta v_{i+1,j} c_{i,j+1} \end{aligned} \tag{41}$$

$$\lambda = \Delta \xi / (\Delta \eta)^2$$

For inner nodes, the coefficients  $A_j, B_j, E_j$  and  $R_j$  are valid. We simplify equation (37) as well as the discretized version of the boundary conditions (39) and (40) for the nodes at the bottom and top of the boundary. The details are provided below:



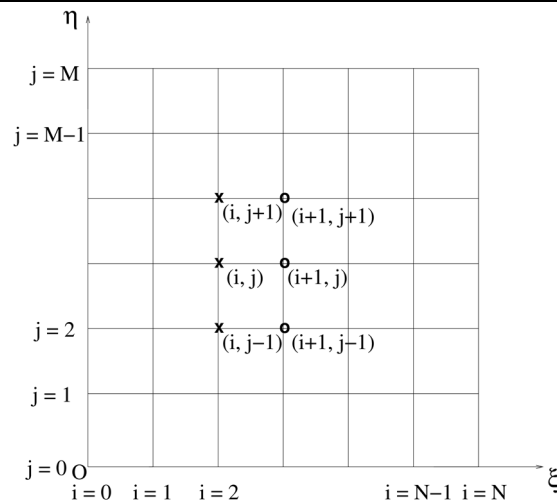
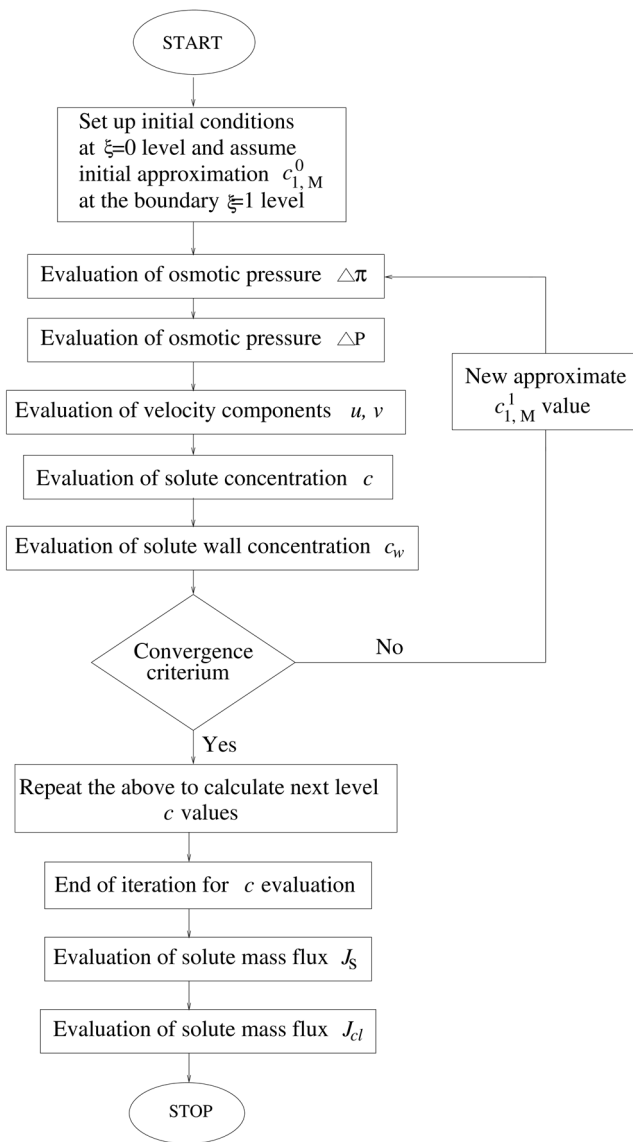
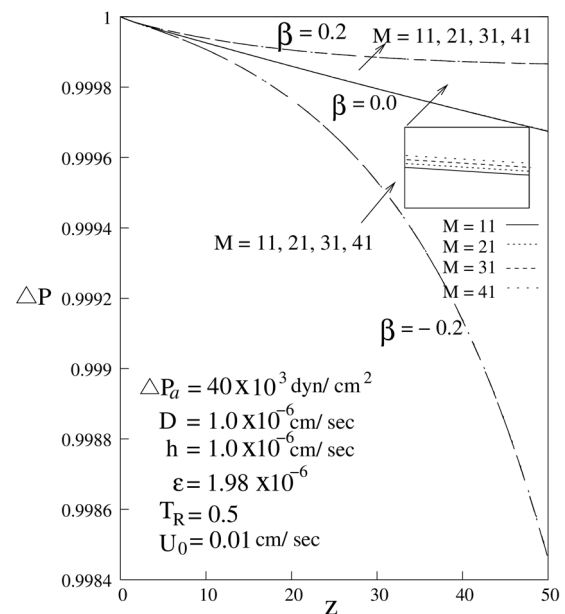


Fig. 2. Details of the grid for the CN scheme around the node (i,j) (Computational domain).



(a)



(b)

Fig. 3. (a) Flowchart showing the iterative method of resolving the flow parameters, (b) Grid independence test: axial hydrostatic pressure ( $\Delta P$ ) distribution at various radial positions.



**Table 1.** Physiological factors for the rat glomerular capillary.

Parameter	Value	Parameter	Value
$L$	$2.5 \times 10^{-2} \text{ cm}$	$r$	$5.0 \times 10^{-4} \text{ cm}$
$k$	$1.33 \times 10^{-8} \text{ to } 1.33 \times 10^{-7} \text{ cm}^3 / \text{ dyn.sec}$	$D$	$3.3 \times 10^{-7} \text{ to } 5.0 \times 10^{-6} \text{ cm}^2 / \text{ sec}$
$h$	$1.0 \times 10^{-6} \text{ to } 7.0 \times 10^{-5} \text{ cm} / \text{ sec}$	$\Delta P_e$	$40 \times 10^3 \text{ to } 55 \times 10^3 \text{ dyn} / \text{ cm}^2$
$c_0$	$6.0 \text{ g} / 100 \text{ ml}$	$U_0$	$0.01 \text{ to } 0.1 \text{ cm} / \text{ sec}$
$\mu$	$0.7 \text{ g} / 100 \text{ ml}$	$b_1$	$2.1 \text{ mmHg} / (\text{g} / 100 \text{ ml})$
$b_2$	$0.16 \text{ mm Hg} / (\text{g} / 100 \text{ ml})^2$	$b_3$	$0.009 \text{ mm Hg} / (\text{g} / 100 \text{ ml})^3$

At  $\eta = 0$ , we have:

$$B_0 c_{i+1,0} + E_0 c_{i+1,1} = R_0 \quad \text{for } j = 0 \tag{42}$$

where  $B_0 = -2\lambda - Pe(u_{i,0} + u_{i+1,0})R(\xi)^2$ ,  $E_0 = 2\lambda$  and  $R_0 = (2\lambda - Pe(u_{i,0} + u_{i+1,0})R(\xi)^2)c_{i,0} - 2\lambda c_{i,1}$ .

At  $\eta = 1$ , we have:

$$c_{i,M} = \frac{4c_{i,M-1} - c_{i,M-2} + 2\Delta\eta Pe R(\xi) Sh c_T}{3 + 2\Delta\eta R(\xi) Sh + 2\Delta\eta Pe (T_R - 1) V_R} \quad \text{if } V_R > 0 \tag{43}$$

and

$$c_{i,M} = \frac{4c_{i,M-1} - c_{i,M-2} + 2\Delta\eta R(\xi) c_T (Sh + Pe(1 - T_R) V_R)}{3 + 2\Delta\eta R(\xi) Sh} \quad \text{if } V_R < 0. \tag{44}$$

The well-known Thomas technique is used to solve the aforementioned set of linear simultaneous equations for  $c_{i,j}$  to obtain the value of  $c$  at each node (grid point) (refer to Fig. 2). At level  $i = 0$ , the values of  $\Delta\pi$ ,  $\Delta P$  and  $c$  are known. We use the following iterative process to obtain the values at  $i = 1$  level. In order to do this, we assume a rough value for  $c$  at the boundary, which is adjusted in accordance with the discretized boundary condition of equations (40) and (37), respectively. The three-point backward difference algorithm [34] was used to derive the new  $c$  value ( $c^1_{i,M}$ ) from equation (40). To obtain the correct value  $c$  at  $i = 1$  level with a tolerance of  $10^{-6}$  the iterative process is continued. The obtained  $c$  value is used to generate  $i = 2$  level  $c$  values in a similar fashion, and the process is then continued up to the level  $i = N$ . The flowchart in Fig. 3(a) illustrates the several phases of the iterative process's algorithm.

### 4.3. Grid Independence Test

To verify the numerical procedure, we discussed the grid independence test. In order to do this, we examine the hydrostatic pressure's axial distribution for various grid point counts in the transverse direction. We varied step size  $\Delta r$  in the  $r$  direction with values of 0.1, 0.2, 0.3, and 0.4 while maintaining a fixed step size  $z = 0.02$  in the  $z$  direction.  $51 \times 11$ ,  $51 \times 21$ ,  $51 \times 31$ , and  $51 \times 41$  nodes are the results of the four runs, respectively. Each of these situations has a C++ code developed for it. The outcomes are displayed in Fig. 3(b). We know that  $51 \times 11$  case is strong enough to forecast the physics of flow, so it is applied in the current investigation. In addition, the maximum difference between the values in each of the four runs is found to be  $10^{-5}$ .

## 5. Results and Discussions

This study presents a model of fluid flow and solute transport within a convergent-divergent permeable tube. The computational findings are obtained by employing the physiological parameters from the Table 1 ([21, 26, 27]). The significant characteristics of the parameters ultrafiltration parameter ( $\epsilon$ ) diffusion coefficient ( $D$ ) and transmittance coefficient ( $T_R$ ) on the variables such as osmotic and hydrostatic pressures, velocities, concentration and clearance of solute are all presented through Figures 4 to 13 and discussed, which are application to solute transfer through the glomerular capillaries. It may be noted that, our results are compared with the previous studies for a particular case of  $\beta = 0$  (i.e., tube is uniform). The slope parameter  $\beta > 0$  and  $\beta < 0$  represent the corresponding results of the diverging and converging tube cases, respectively (see Fig. 1). In this analysis, we have indicated the dimensional quantity values in figures, since the dimensionless terms such as ultrafiltration parameter ( $\epsilon$ ), Peclet number ( $Pe$ ), and Sherwood number ( $Sh$ ) comprise the parameters  $h$ ,  $T_R$ ,  $D$  and  $k$ .

### 5.1. Hydrostatic Pressure ( $\Delta P$ ) and Osmotic Pressure ( $\Delta\pi$ )

The hydrostatic and osmotic pressure distributions for uniform, converging, and diverging tube cases with various parameter values are depicted in Figs. 4 to 8. The distance along the tube is represented by the  $z$  axis. The  $r$  axis displays the hydrostatic and osmotic pressures. The  $\Delta P$  profile decays along the axial distance. The parameter  $\Delta\pi$  increases along the glomerular capillary, as depicted in the figures. The profile of  $\Delta\pi$  is determined by (1) its value at the one end of the glomerular capillary where filtration begins,  $\pi$ , determined by systemic plasma solute concentration, and (2) the degree of the increase in solute concentration along the capillary as a result of losing colloid-free solution as ultrafiltrate. Figure 4 shows the distribution of the hydrostatic and osmotic pressures with slope parameter  $\beta$ . From Figs. 4(a) and 4(b), it is noteworthy to observe that there is a variation between  $\Delta P$  and  $\Delta\pi$  values, at any axial position, leads to the fluid movement/ultrafiltration pressure. Referring to Fig. 4(a), it can be seen that the value of  $\Delta P$  is larger for a diverging tube case and less for a converging tube case when compared to the values of a uniform tube case. In the case of a uniform tube, the  $\Delta P$  drops linearly along the axis. The decrease in  $\Delta P$  for convergent (divergent) tubes is comparably quicker (slower) than the decline in uniform tubes as slope parameter ( $\beta$ ) rises. As a result, the slope parameter significantly alters the hydrostatic pressure's evolution along the tube's length. Along the axis, the osmotic pressure rises in a nonlinear manner. It is observed that the value of  $\Delta\pi$  is more for divergent tube case and less for convergent tube case as compared to the values of a straight tube case (Fig. 4(b)). This indicates that there is a significant influence of slope parameter  $\beta$  on  $\Delta P$  and  $\Delta\pi$ .



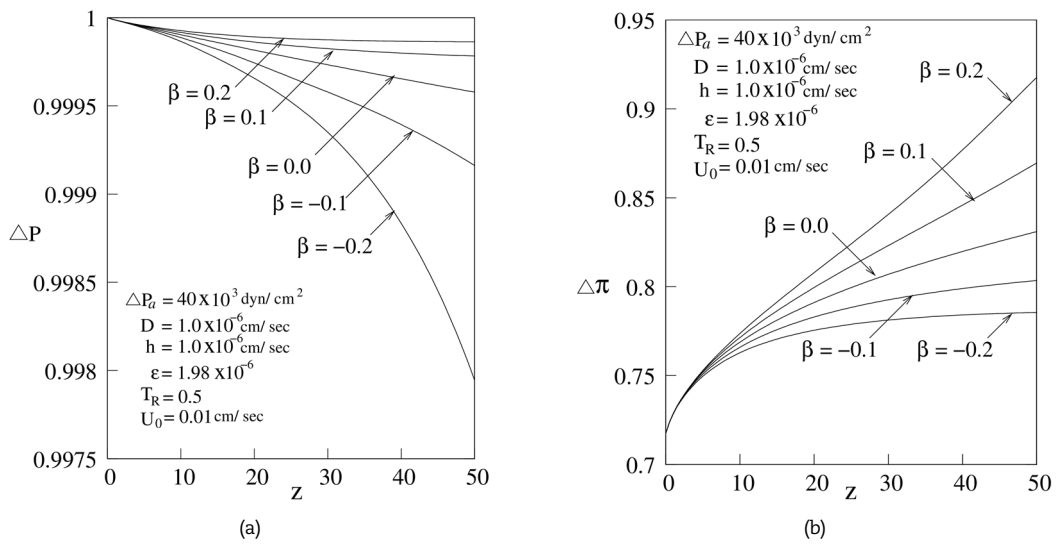


Fig. 4. Distribution of  $\Delta P$  and  $\Delta \pi$  for different  $\beta$  values.

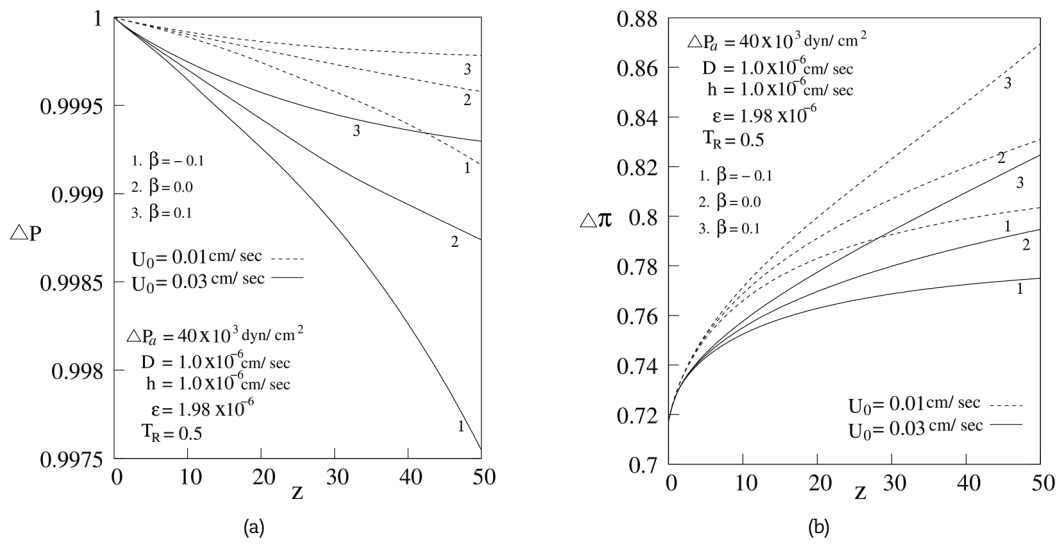


Fig. 5. Distribution of  $\Delta P$  and  $\Delta \pi$  for different  $U_0$ .

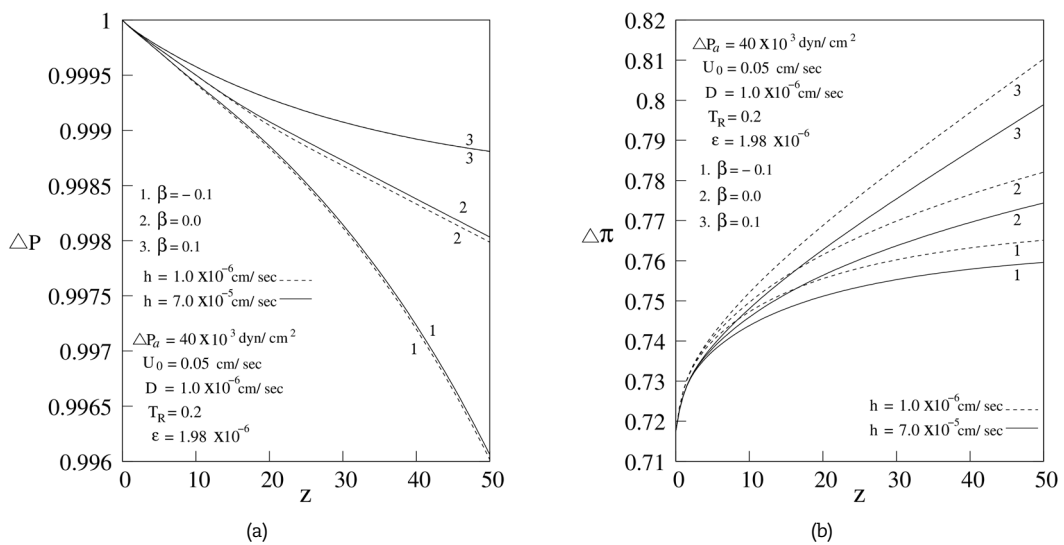


Fig. 6. Distribution of  $\Delta P$  and  $\Delta \pi$  for different  $h$ .



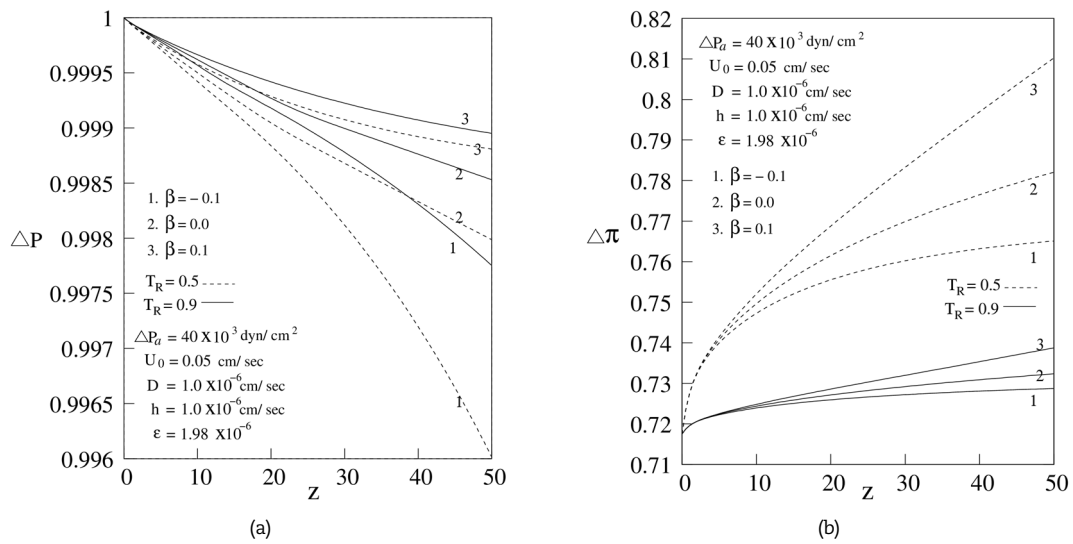


Fig. 7. Distribution of  $\Delta P$  and  $\Delta \pi$  for different  $T_R$ .

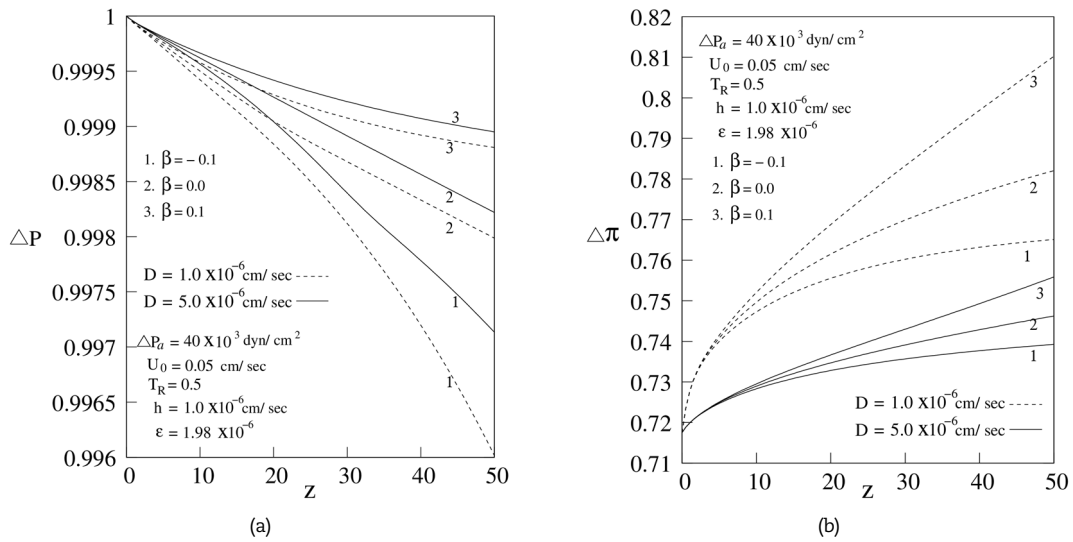


Fig. 8. Distribution of  $\Delta P$  and  $\Delta \pi$  for different  $D$ .

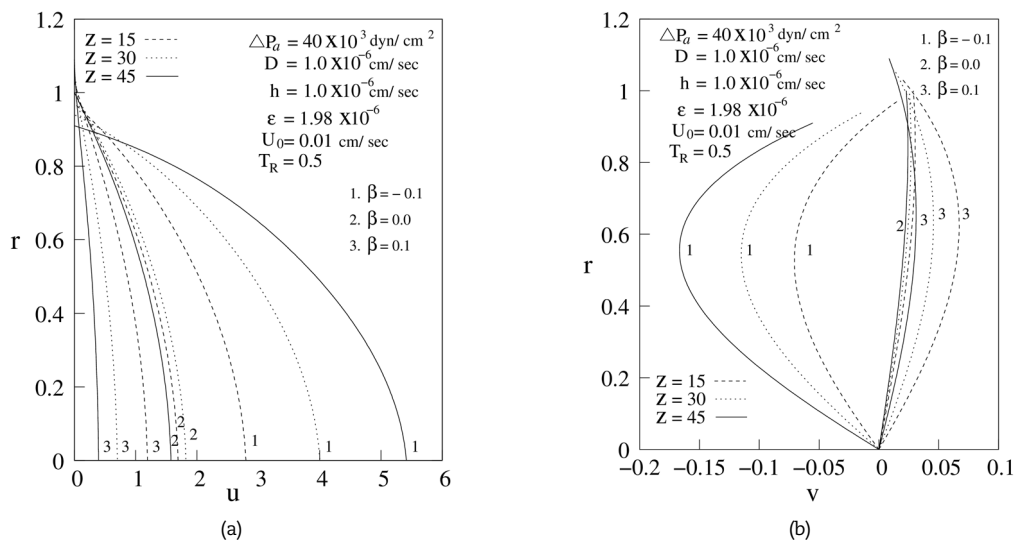


Fig. 9. Axial and radial velocity at different cross-sections along the axis for various  $\beta$  values.



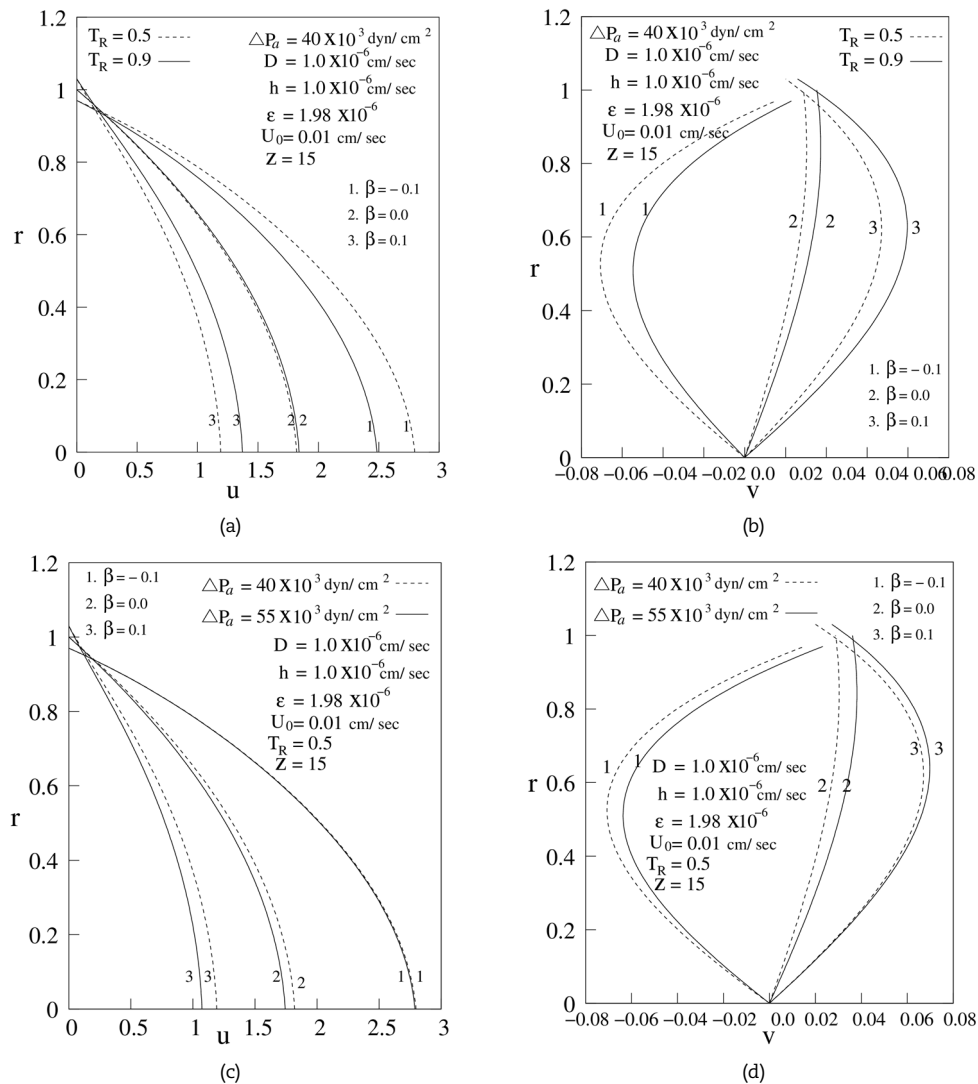


Fig. 10. Axial and radial velocity for different  $T_R$  and  $\Delta P_a$  values.

Figure 5 exhibits the distribution of  $\Delta P$  and  $\Delta \pi$  with reference to the initial average velocity  $U_0$ . In the downstream of the capillary, the hydrostatic pressure and osmotic pressure decreases with increasing  $U_0$ , in all three cases of slope parameter which agrees with previous studies (Chaturani and Ranganatha [30]). The variation of the hydrostatic pressure  $\Delta P$  and osmotic pressure  $\Delta \pi$  with wall permeability  $h$  is presented in Fig. 6. An increase in solute transport through the permeable wall is implied by the rising values of  $h$ . According to Fig. 6(a), the hydrostatic pressure has a very minimal influence as the value of  $h$  increases. In Fig. 6(a), it is observed that the osmotic pressure decreases in along the axial direction with rise in  $h$ .

Figure 7 illustrates the effect of transmittance coefficient  $T_R$  on  $\Delta P$  and  $\Delta \pi$ . Figure 7(a) shows that the increased hydrostatic pressure values due to increase in the transmittance coefficient  $T_R$  and Fig. 7(b) represents that the osmotic pressure decreases with rise in  $T_R$ . Figure 8 depicts the effect of the diffusion coefficient  $D$  on  $\Delta P$  and  $\Delta \pi$ . As the diffusion coefficient  $D$  rises, the hydrostatic pressure ( $\Delta P$ ) also rises (see Fig. 8(a)). As depicted in Fig. 8(b), the osmotic pressure at the tube's output decreases when the diffusion coefficient  $D$  increases. Therefore, it is observed that the  $\Delta P$  is not much affected by the values of  $h$ ,  $T_R$  and  $D$ , where as the osmotic pressure significantly affected by these parameters as discussed above, in three cases of slope parameter  $\beta$ .

5.2. Axial Velocity  $u(r, z)$  and Radial Velocity  $v(r, z)$

Figures 9 and 10 show the behavior of velocities  $u(r, z)$  and  $v(r, z)$  for various parameters  $\beta$ ,  $T_R$  and  $\Delta P_a$  at different  $z$ -locations noted on the figures. Figure 9 depicts the influence of slope parameter ( $\beta$ ) on axial velocity ( $u(r, z)$ ) and radial velocity ( $v(r, z)$ ) at various axial positions of the tube. Figure 9(a) shows that the velocity ( $u(r, z)$ ) profile is parabolic and has a greatest value at the tube's axis. It is important to note that the axial velocity is zero near the tube's wall for straight case. The  $u$ -velocity is more for convergent tube compared with uniform and divergent tube cases. From Fig. 9(b), the  $v$ -velocity is zero on the axis of the tube. It is seen that the negative  $v(r, z)$  occur for convergent tube and positive  $v$  for uniform and divergent tubes. The  $v$ -velocity has maximum value near  $r = 0.8$ , for straight tube case when  $z = 15$ . In the case of divergent tubes, the maximum  $v(r, z)$  is obtained near  $r = 0.6$ . For convergent tubes, minimum of  $v(r, z)$  is obtained at  $r = 0.5$ .

Figure 10 shows the influence of  $T_R$  and  $\Delta P_a$  on velocity  $u(r, z)$  and velocity  $v(r, z)$ . The velocity  $u(r, z)$  decreases for convergent tube and increases for uniform and divergent tubes for different values of  $T_R$ . As  $\Delta P_a$  rises the axial velocity diminishes for uniform, convergent and divergent tubes at  $z = 15$  location, but  $u(r, z)$  rises for convergent and decreases for



uniform and divergent tube cases. From the velocity  $v(r, z)$  at the wall calculated at two different locations  $z = 15$  and  $z = 45$ , it is observed that velocity  $v(r, z)$  at the wall increases, with varying  $T_R$  and  $\Delta P_a$ .

**5.3. Concentration Profiles  $c(r, z)$**

The concentration profiles for various  $T_R$  and  $h$  values at  $z = 15$  is depicted through figure 11, with different slope parameter  $\beta$ . One can see that,  $c(r, z)$  increases with  $r$  from the capillary axis to the wall. This signifies that the capillary wall does not transport all of the solute across the wall. Due to the ultrafiltration process, the concentration  $c(r, z)$  rises with tube axis. The solute concentration is more for divergent tubes than the uniform and convergent tube cases. In general, the solute concentration  $c(r, z)$  increases with  $r$  from axis of tube to the wall. In all three situations, the solute concentration falls down along the tube's length for various  $h$  and  $T_R$ . There is no transport of solute over the tube wall when  $h = 0$  and  $T_R = 0$  (Deen et al. [18]). Due to an increase in osmotic pressure, the filtration velocity slows down at the end of the capillary. This slows down the velocity  $v(r, z)$  inside the tube, which slows down the solute transport toward the capillary wall.

Figure 12 shows the variation of the solute concentration  $c(r, z)$  with the radial axis for different values of the ultrafiltration parameter and diffusion coefficient. It is shown that when parameter  $\varepsilon$  increases, the solute concentration rises, indicating an increase in solute per unit volume at the capillary wall. The concentration of the solute near the axis decreases as  $D$  increases in all three instances of the capillary's geometry. The concentration  $c(r, z)$  rises along the radial axis when  $\varepsilon$  is present for a given  $D$ . It is accurate to say that there is solute movement through the wall by the process of diffusion when zero ultrafiltration coefficient ( $\varepsilon = 0$ ). That is, at cross section  $z = 15$ , the radial concentration profile significantly decreases from the initial constant value ( $c_0 = 1$ ) to zero.

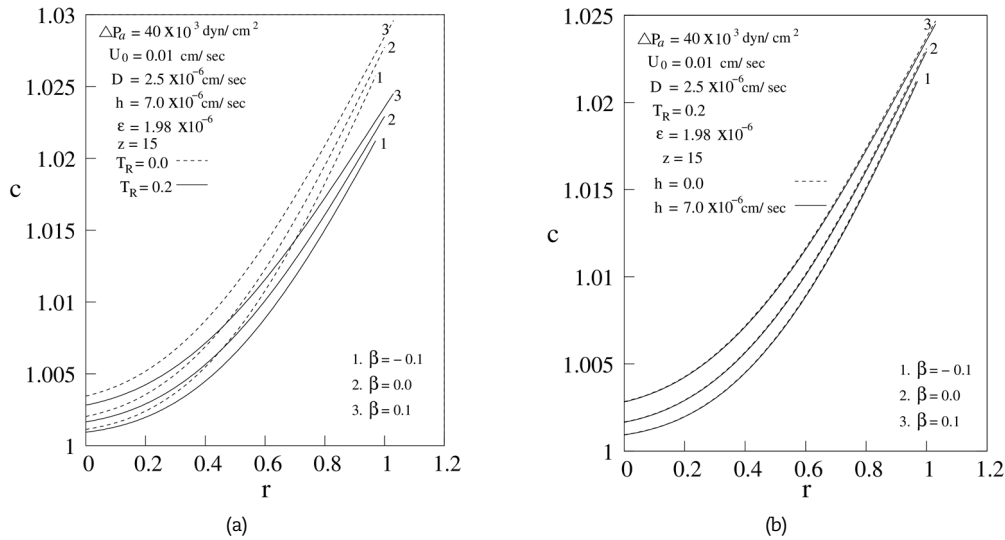


Fig. 11. Distribution of solute concentration for different  $T_R$  and  $h$  values with  $r$  at different axial positions.

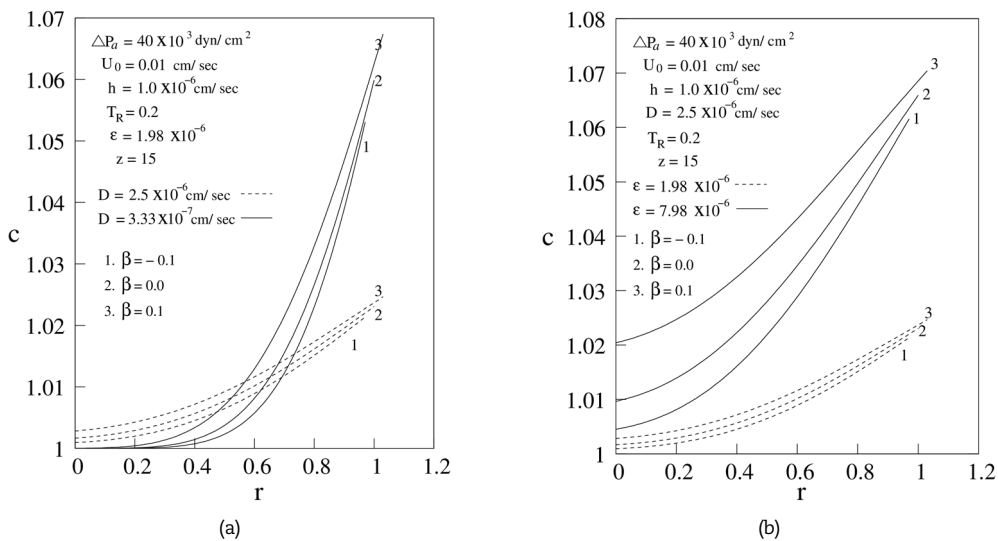


Fig. 12. Distribution of solute concentration for different  $D$  and  $\varepsilon$  values with  $r$  at different axial positions.



**Table 2.**  $J_c$  for  $U_0 = 0.01$  cm / sec,  $T_R = 0.2$ ,  $\Delta P_a = 40 \times 10^3$  dyn /  $cm^2$  and  $D = 1 \times 10^{-6}$   $cm^2$  / sec.

$\beta$	$\varepsilon = 7.98 \times 10^{-7}$		$\varepsilon = 1.98 \times 10^{-6}$	
	Sh = 0.005	Sh = 0.035	Sh = 0.005	Sh = 0.035
-0.1	0.144771	0.243727	0.276755	0.385881
0.0	0.142279	0.2425	0.260059	0.372307
0.1	0.137716	0.239662	0.234352	0.350477

**Table 3.**  $J_c$  for  $U_0 = 0.01$  cm / sec,  $T_R = 0.5$ ,  $\Delta P_a = 40 \times 10^3$  dyn /  $cm^2$  and  $D = 1 \times 10^{-6}$   $cm^2$  / sec.

$\beta$	$\varepsilon = 7.98 \times 10^{-7}$		$\varepsilon = 1.98 \times 10^{-6}$	
	Sh = 0.005	Sh = 0.035	Sh = 0.005	Sh = 0.035
-0.1	0.356807	0.45965	0.751954	0.87137
0.0	0.353706	0.458241	0.724632	0.848982
0.1	0.346763	0.453133	0.683499	0.813607

**5.4. Wall Concentration ( $c_w$ )**

Figure 13 depicts the wall concentration  $c_w$  variation in uniform, divergent, and convergent tubes with various  $h$ ,  $T_R$  and  $\varepsilon$ . From these figures, we can see that the effect of  $\beta$  on the variation of wall concentration along axial direction. It has been observed that the tube slope parameter has a greater impact on  $c_w$ . The tube slope parameter has been found to have a greater impact on  $c_w$ . When compared to the values of a straight tube case, it is observed that the value of  $c_w$  is higher for the divergent tube case and lower for the convergent tube case. Along the tube's axial length, there is a rise in wall concentration. As  $h$  and  $T_R$  rise, we see a drop in the wall solute concentration (Fig. 13(a), 13(b)). Figure 13(c) shows the relationship between wall concentration and axial distance at various values of ultrafiltration parameter  $\varepsilon$ . The concentration at the wall rises as  $\varepsilon$  rises, as would be expected (see Fig. 13(c)).

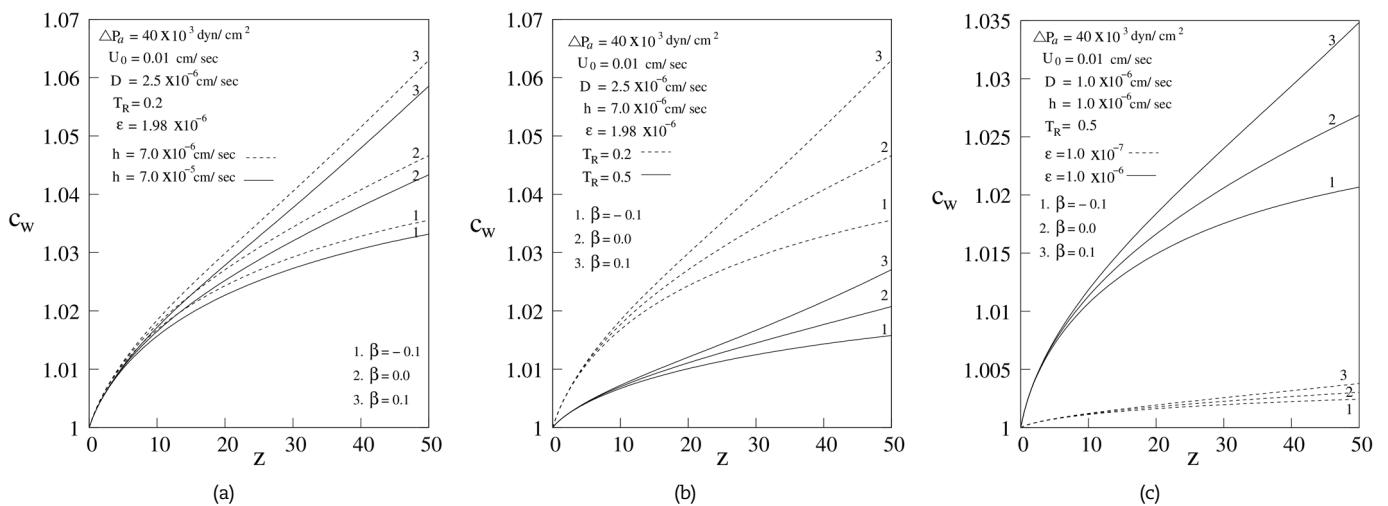


**Fig. 13.** Concentration  $c(z)$  for different  $h$ ,  $T_R$ , and  $\varepsilon$  values with  $z$ .

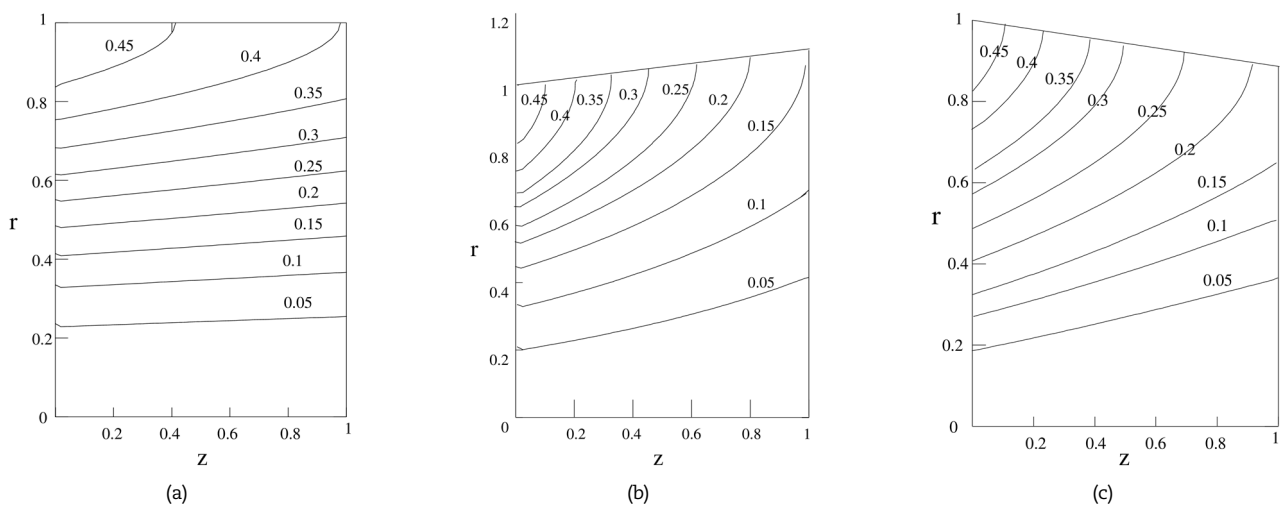


**Fig. 14.** Distribution of streamline for uniform tube ( $\beta = 0.0$ ), diverging tube ( $\beta = 0.1$ ) and converging tube ( $\beta = -0.1$ ).



**Table 4.** Comparison of the current study and previous results for the limiting case of  $\beta = 0.0, z = 25$  for hydrostatic pressure ( $\Delta P$ ) along the tube length.

$U_0$	Ref. [30]	Ref. [26]	Ref. [27]	Present work
0.01	0.999741	0.999741	0.999741	0.999741
0.03	0.999207	0.999208	0.999208	0.999208
0.10	0.997012	0.996988	0.996988	0.996988

**Table 5.** Comparison of the current study and previous results for the limiting case of  $\beta = 0.0, z = 25$  for wall concentration ( $c_w$ ) along the tube length.

$T_R$	Ref. [30]	Ref. [26]	Ref. [27]	Present work
0.0	1.054540	1.0545	1.0545	1.05476
0.5	1.033321	1.0333	1.0333	1.03352
0.7	1.021749	1.02175	1.02175	1.02191

### 5.5. Total solute clearance ( $J_c$ )

Tables 2 and 3 display the total solute clearance result  $J_c$  with the impacts of  $\beta$ ,  $T_R$ ,  $\varepsilon$  and  $h$ . It is obvious that the solute clearance is significantly impacted by the slope parameter ( $\beta$ ). In other words, relative to the figures for a straight tube case, the solute clearance is higher for convergent cases and lower for diverging cases. With a rise in transmittance coefficient, the solute clearance increases significantly. By raising ultrafiltration parameter ( $\varepsilon$ ) and wall permeability ( $h$ ), the value of  $J_c$  is enhanced.

### 5.6. Stream lines

Figure 14 displays the streamline graphs for the three situations of the slope parameter ( $\beta$ ). These illustrations show how the flow pattern of uniform, diverging, and converging tube examples behaves. Due to the permeability nature of the tube and the fact that the bulk flow is reduced at the exit in three instances involving uniform, diverging, and converging tubes, the streamlines pattern migrated in the direction of the wall.

### 5.7. Validation and Accuracy

The numerical model utilized in the current study is validated using previously published research works ([26, 27, 30]). The hydrostatic pressure ( $\Delta P$ ) for the uniform tubular case ( $\beta = 0.0$ ) are calculated at  $z = 25$ , with various values of the mean axial velocity ( $U_0$ ), and a very good agreement is obtained, which is shown in Table 4. Additionally, Table 5 provides the wall concentration ( $c_w$ ) for the uniform tubular case ( $\beta = 0.0$ ) at  $z = 25$ , with different transmittance coefficient ( $T_R$ ) values. Table 5 demonstrates that the findings of the current analysis are in good agreement with the published work in the limited situations.

## 6. Conclusions

To our knowledge, the model provided in this paper is the first mathematical model of fluid and solute transport in glomerular capillaries that takes into consideration capillary wall non-uniformity and permeability properties. It is significant to note from the results that the hydrostatic pressure loss is rather minimal and that some earlier models expected it to be constant. The study's new aspects include its analysis of solute transfer via permeable tubes as well as converging-diverging boundaries, specifically with regard to the flow in glomerular capillaries. The results are found for hydrostatic and osmotic pressures, velocities, concentration and solute clearance, showing the effects of the non-uniformity and various other parameters. The results meet the necessary criteria of yielding the prior research' results ([26, 27, 30]) in the limiting case with the slope parameter approaching to zero. Based on the findings of the present study, the following conclusions can be drawn:

- There is a linear decline in hydrostatic pressure, and a nonlinear rise in osmotic pressure along the axial direction, in all three cases of the slope parameter ( $\beta$ ). As  $h$ ,  $T_R$  and  $D$  increase, the hydrostatic pressure does not significantly change, but the osmotic pressure decreases at the tube's end with an increase in  $h$ ,  $T_R$  and  $D$ .
- The axial velocity is more for convergent tube case compared with uniform and divergent tube cases. The radial velocity is more for divergent tube case compared with uniform and convergent tube cases.
- As compared to uniform and convergent tube cases, divergent tube cases have a greater concentration of solute. It has been observed that the parameters  $T_R$ ,  $h$ ,  $D$  and  $\varepsilon$  have an impact on concentration profiles.
- The value of  $c_w$  is more for divergent tube case and less for convergent tube case as compared to the values of straight tube case. A decrease in wall concentration is observed with an increase in  $h$ , and  $T_R$ . There is an increasing difference between these two results as  $\varepsilon$  rises. As  $\beta$ ,  $T_R$ ,  $h$ , and  $\varepsilon$  increase, so does the total solute clearance  $J_c$ .
- The flow behavior along the permeable tube wall is described by the streamlines for uniform, converging and diverging tubes.

It should be highlighted that the current research only considers mass transfer in convergent-divergent tubes. However, in actual physiological circumstances, capillaries also have a wavy wall. Therefore, the current model may be made more realistic by including a wavy tube border.

### Author Contributions

M. Varunkumar formulated the concept, began the work, and proposed the model; P. Muthu carried out the approach and looked at the manuscript's theoretical justification; S. Srinivas analyzed the findings; and all the authors discussed, reviewed, and gave their approval to the manuscript's final document.

### Acknowledgments

We want to express our sincere thanks to the reviewers for taking the necessary time and effort to review the article. We sincerely thank you for your insightful comments and advice, which helped us to enhance the quality of the manuscript.



## Conflict of Interest

The authors declared no conflicts of interest concerning the research, authorship, and publication of this article.

## Funding

The authors received no financial support for the research, authorship, and publication of this article.

## Data Availability Statements

The datasets generated and/or analyzed during the current study are available from the corresponding author on reasonable request.

## References

- [1] Apelblat, A., Katchasky, A.K., Silberberg, A., A mathematical analysis of capillary tissue fluid exchange, *Biorheology*, 11, 1974, 1-49.
- [2] Palatt, J.P., Henry S., Roger, I.T., A hydrodynamical model of a permeable tubule, *Journal of Theoretical Biology*, 44, 1974, 287-303.
- [3] Brenner, B.M., Troy, J.L., Daugharty, T.M., Deen, W.M., Dynamics of glomerular ultrafiltration in the rat. II. Plasma flow dependence of GFR, *American Journal of Physiology*, 223, 1972, 1184-1190.
- [4] Keener, J., Sneyd, J., *Mathematical Physiology*, 2nd Edition, Springer, 2009.
- [5] Guyton, A.C., John, E.H., *Text Book of Medical Physiology*, 11th Edition, Elsevier Saunders Publishing, 2011.
- [6] Brenner, B.M., Troy, J.L., Daugharty, T.M., Deen, W.M., Dynamics of glomerular ultrafiltration in the rat. II. Plasma flow dependence of GFR, *American Journal of Physiology* 223, 1972, 1184-1190.
- [7] Brenner, B.M., Baylis, C., Deen, W.M., Transport of molecules across renal glomerular capillaries, *Physiological Reviews*, 56, 1978, 502-534.
- [8] Martin, R.P., Susan, E.Q., Melanie, P.H., Lance, D.D., The glomerulus: The sphere of influence, *Clinical Journal of the American Society of Nephrology*, 9, 2014, 1461-1469.
- [9] Misra, J.C., Ghosh, S.K., A mathematical model for the study of blood flow through a channel with permeable walls, *Acta Mechanica*, 122, 1997, 137-153.
- [10] Moustafa, E., Blood flow in capillary under starling hypothesis, *Applied Mathematics and Computation*, 149, 2004, 431-439.
- [11] Yuan, S.W., Finkelstein, A.B., Laminar pipe flow with injection and suction through a porous wall, *Transactions of the American Society of Mechanical Engineers*, 78, 1956, 719-724.
- [12] Kedem, O., Katchalsky, A., A physical interpretation of the phenomenological coefficients of membrane permeability, *Journal of General Physiology*, 45, 1961, 143-179.
- [13] Deen, W.M., Robertson, C.R., Brenner, B.M., A model of glomerular ultrafiltration in the rat. *American Journal of Physiology*, 223, 1972, 1178-1183.
- [14] Marshall, E.A., Trowbridge, E.A., A mathematical model of the ultrafiltration process in a single glomerular capillary, *Journal of Theoretical Biology*, 48, 1974, 89-412.
- [15] Papenfuss, H.D., Gross, J.F., Analytical study of the influence of capillary pressure drop and permeability on glomerular ultrafiltration, *Microvascular Research*, 16, 1978, 59-72.
- [16] Papenfuss, H.D., Gross, J.F., Transcapillary exchange of fluid and plasma proteins, *Biorheology*, 24, 1987, 319-335.
- [17] Salathe, E.P., Mathematical studies of capillary tissue exchange, *Bulletin of Mathematical Biology*, 50, 1988, 289-311.
- [18] Deen, W.M., Robertson, C.R., Brenner, B.M., Concentration polarization in an ultrafiltering capillary, *BioPhysical Journal*, 14, 1974, 412- 431.
- [19] Ross, M.S., A mathematical model of mass transport in a long permeable tube with radial convection, *Journal of Fluid Mechanics*, 63, 1974, 157-175.
- [20] Tyagi, V.P., Abbas, M., An exact analysis for a solute transport, due to simultaneous dialysis and ultrafiltration, in a hollow-fibre artificial kidney, *Bulletin of Mathematical Biology*, 49, 1987, 697-717.
- [21] Chaturani, P., Ranganatha, T.R., Flow of Newtonian fluid in non-uniform tubes with variable wall permeability with application to flow in renal tubules, *Acta Mechanica*, 88, 1991, 11-26.
- [22] Layton, A.T., Layton, H.E., A computational model of epithelial solute and water transport along a human nephron, *PLoS Computational Biology*, 15(2), 2019, e1006108.
- [23] Pstras, L., Waniewski, J., Lindholm, B., Transcapillary transport of water, small solutes and proteins during hemodialysis, *Scientific Reports*, 10, 2020, 18736.
- [24] Waniewski, J., Pietribiasi, M., Pstras, L., Calculation of the Gibbs-Donnan factors for multi-ion solutions with non-permeating charge on both sides of a permselective membrane, *Scientific Reports*, 11, 2021, 22150.
- [25] Radhakrishnamacharya, G., Peeyush, C., Kaimal, M.R., A hydrodynamical study of the flow in renal tubules, *Bulletin of Mathematical Biology*, 43, 1981, 151-163.
- [26] Varunkumar, M., Muthu, P., Fluid flow and solute transfer in a tube with variable wall permeability, *Zeitschrift für Naturforschung A*, 74, 2019, 1057-1067.
- [27] Varunkumar, M., Muthu, P., Fluid flow and solute transfer in a permeable tube with influence of slip velocity, *An Interdisciplinary Journal of Discontinuity, Nonlinearity, and Complexity*, 9, 2020, 153-166.
- [28] Radhakrishnamacharya, G., Muthu, P., Varunkumar, M., Mathematical Model of Fluid Flow and Solute Transfer in a Permeable Channel with Slip Velocity at the Boundaries, *Proceedings of National Academy Sciences, India, Section-A Physical Sciences*, 91, 2021, 611-622.
- [29] Krishnaprasad, J.S.V.R., Chandra, P., *Low Reynolds number flow in a channel with varying cross section and permeable boundaries*, In: *Bio Mechanics*, New Delhi, WillEastern Ltd, 1988.
- [30] Chaturani, P., Ranganatha, T.R., Solute transfer in fluid in permeable tubes with application to flow in glomerular capillaries, *Acta Mechanica*, 96, 1993, 139-154.
- [31] Regirer, S.A., Quasi one-dimensional model of transcapillary filtration, *Journal of Fluid Dynamics*, 10, 1975, 442-446.
- [32] Shetinger, U.R., Prabhu, H.J., Ghista. D.N., Blood Ultrafiltration: A Design Analysis, *Medical and Biological Engineering and Computation*, 15, 1977, 32-38.
- [33] John, D.A.Jr., *Computational Fluid Dynamics - The Basics with Applications*, McGraw-Hill, 1995.
- [34] Chung, T.J., *Computational Fluid Dynamics*, 2nd Edition, Cambridge University Press, 2010.

## ORCID iD

M. Varunkumar  <https://orcid.org/0000-0003-1185-7133>

P. Muthu  <https://orcid.org/0000-0001-8582-1753>

S. Srinivas  <https://orcid.org/0000-0002-3666-981X>



© 2023 Shahid Chamran University of Ahvaz, Ahvaz, Iran. This article is an open access article distributed under the terms and conditions of the Creative Commons Attribution-NonCommercial 4.0 International (CC BY-NC 4.0 license) (<http://creativecommons.org/licenses/by-nc/4.0/>).



**How to cite this article:** Varunkumar V., Muthu P., Srinivas S. Mathematical Model of Fluid Flow and Solute Transport in Converging-diverging Permeable Tubes, *J. Appl. Comput. Mech.*, 9(4), 2023, 900-914.  
<https://doi.org/10.22055/jacm.2023.41829.3818>

**Publisher's Note** Shahid Chamran University of Ahvaz remains neutral with regard to jurisdictional claims in published maps and institutional affiliations.

